Appendix 2

Appendix 2.1 Photosynthesis

A.2.1.1 Light Harvesting and Photosystem II (PSII)

The central structure for light energy conversion is the photosystem, a macromolecular pigment-protein complex integral to the thylakoid membrane. Photosystem II (PS II) consists of two key components, a peripheral antenna containing chlorophyll a (Chl *a*) and other pigment molecules that absorb light, and a reaction center at the core of the complex (Govindjee et al. 2010). The light absorbed in the antenna is transferred to the reaction center (Fig. 1, red arrows) where an electron in the Chl *a* molecule becomes excited and the first steps of electron transport occur (Fig. 1, black arrows). In eukaryotic phytoplankton, the light harvesting complex II antenna (labeled LHC-II in Fig. 1a) is integral to the thylakoid, just as the core is, but in most prokaryotes, the phycobilisome antenna rests on top of the thylakoid membrane (Fig. 1b). While the core complex is highly conserved among all classes of photosynthetic organisms, the antenna are diversified in terms of their structure and the types of pigments they bind (Ballottari et al. 2012).

After the electron in the reaction center becomes excited it's transferred to the plastoquinone pool (PQ) and on down the electron chain to the final electron acceptor NADP+. Along the way, energy from the electrons is used to push protons to the lumen side of the thylakoid membrane. With continued electron transfer down the chain, protons accumulating in the lumen build up a cross-membrane potential that is subsequently used to power ATP synthesis. Meanwhile, the electron originally lost from Chl *a* in the reaction center is replaced by an electron extracted from water; four photons are required to remove four electrons from two water molecules to produce one molecule of oxygen (Govindjee et al. 2010).

A.2.1.2 Photoprotection and stress

PSII is the only photosystem that catalyzes the splitting of water and the production of oxygen in photosynthetic organisms. With this distinction also comes great danger when the cell absorbs more energy than it can use to power C- fixation. In that case, the entire electron chain may back-up resulting in the release of free electrons that combine with oxygen to produce oxygen radicals that damage the PSII proteins (Vass et al. 1992, Clarke et al. 1993). To avoid this situation, photosynthetic cells have several built-in "electron valves" (e.g. Bailey et al. 2008, Zehr and Kudela 2009). One of the most effective occurs at the point where light energy is harvested; instead of being funneled to the reaction center, it can be dissipated as heat by the accessory pigments in the antenna (Ballottari et al. 2012). In diatoms, this involves the action of carotenoid xanthophyll cycle pigments (Nymark et al. 2009). This radically slows the flow of electrons through the electron transport chain and decreases the efficiency of the conversion of

light energy to ATP, also known as the quantum yield of PSII (or yield). The decrease in yield occurs in all photosynthetic cells in response to any stressor that affects C-fixation and can be measured reliably with an instrument that measures variable fluorescence.

A.2.1.3 PSII efficiency and fluorescence

In addition to generating ATP and heat, light energy can be dissipated as fluorescence. In an optimally functioning photosynthetic cell, up to 90% of the harvested light energy is used to excite electrons in the PSII reaction centers and very little is dissipated as heat or fluorescence. As the cell becomes more stressed, less of the energy is used for photochemistry and more is dissipated as heat. The amount of energy that goes into photochemistry can be measured by channeling it into fluorescence. This is accomplished by closing all reaction centers in the cell at once; the resulting increase in fluorescence corresponds to the amount of light energy that would otherwise be used to excite electrons (Fig. 2). By subtracting the baseline fluorescence (F_o) from this maximal fluorescence (F_m), one arrives at variable fluorescence (F_m-F_o=F_v) which provides a direct estimate of the quantum yield of PSII. Because the architecture of the PSII core, and therefore fluorescence emission, are highly conserved, the range in variable fluorescence is similar across all photosynthetic taxa. When cells are stressed, yield and variable fluorescence rapidly decline. Typically, F_v is expressed as a fraction of F_m. This quotient, F_v/F_m, varies from 0 to about 0.65 in marine phytoplankton depending on the baseline fluorescence reading (Kromkamp and Forster 2003). Phycobilin-containing cyanobacteria tend to have a slightly greater baseline reading (F_0), therefore F_v/F_m typically ranges between 0-0.5 (Cambell et al. 1998).

Variable fluorescence is widely used in phytoplankton ecology to document environmental stress such as toxicity from herbicides (Fai et al. 2007, Choi et al. 2012), nutrient limitation (Geider et al. 1993, Young and Beardall 2003, Berg et al. 2008, Kudela 2008, Parkhill et al. 2012), high light or UV exposure (Six et al. 2004, 2007, Berg et al. 2011) and oxidative stress (Drabkova et al. 2007), to mention a few.

A.2.1.4 Photoacclimation

Dissipation of excess light energy as heat (or fluorescence) are short-term responses. A photosynthetic cell can also acclimate to changes in irradiance over the longer term by adjusting the size its peripheral antenna to capture more or less energy. Under persistent high light, the cell will acclimate by shedding Chl *a* in order to decrease its antenna size. Photoacclimation occurs on the order of hours and is not only affected by changes in irradiance, but also by changes in nutrients and temperature. With constant irradiance, a decrease in nutrient concentration will have the same physiological effect as an increase in light intensity because the energy capture will be in excess of C fixation as the cell slows its growth. To avoid photoinhibiton (loss of photosynthetic function due to PSII damage in excess of cell's capacity of repair) under

persistent nutrient limitation, cells will decrease their Chl *a* cell^{-1} (LaRoche et al. 1993, Graziano et al. 1996). With constant irradiance and nutrient concentration, an increase in temperature will increase the growth rate of phytoplankton and therefore their energy needs. To compensate, the cell will increase its antenna size and Chl *a* cell^{-1} (Geider 1987). Changes in Chl *a* cell^{-1} as a function of irradiance, nutrient concentration and temperature substantially influences the C:chl *a* ratio (C:Chl) of the cell. and decreases exponentially with increased temperature (and growth rate) at constant light level (Fig. 3).

Appendix 2.2 Carbon Fixation

A.2.2.1 The Calvin Cycle

As mentioned above, photochemistry leads to a) the build-up of a proton-motive force and subsequent production of ATP via photophosphorylation and b) reducing power in the form of NADPH. The link between C fixation (the process of attaching gaseous CO_2 to a C skeleton) and photochemistry becomes evident when we examine the energetics of C fixation. It takes electrons from two NADPH carriers and 3 ATP molecules to fix a single CO_2 molecule in the Calvin cycle (Fig. 3). Therefore, C fixation would grind to a halt without a continuous supply of reducing power and ATP from the light reactions (Fig. 3).

The rate-limiting step in C fixation is the Ribulose-1,5- Bisphosphate Carboxylase/Oxygenase (Rubisco) enzyme, which catalyzes the first step in the Calvin cycle. This is because Rubisco is notoriously slow and catalyzes 3 molecules per second compared with 1000 molecules per second for a typical reaction. To make up for this the cell has to produce large quantities of the enzyme. The cell also has to make sure that all the Rubisco enzymes are saturated with CO_2 to prevent oxygen from binding to its active site. This may be problematic for marine phytoplankton that live in habitats where the concentration of CO_2 found in seawater can limit phytoplankton C fixation (Riebesell et al. 1993). To deal with this issue, most marine phytoplankton evolved what is collectively known as C concentrating mechanisms (CCM). Rather than depend on the diffusion of CO_2 across the plasma membrane, phytoplankton actively take up bicarbonate (HCO_3^-) occurring at a concentration of 2 mmol/L in seawater. Inside the cell, HCO_3^- is converted to CO_2 in close proximity to Rubisco in order to saturate the enzyme reaction (Krooth et al. 2008).

A.2.2.2 Beta carboxylation

Phytoplankton can also directly fix HCO_3^- to organic C. This pathway, mediated by the enzymes phosphoenolpyruvate carboxylase (PEPC) and pyruvate carboxylase (PYC) catalyze the reaction of HCO_3^- to either phosphoenolpyruvate or pyruvate, respectively, to form oxaloacetate (OAA). These enzymes are primarily targeted to the mitochondria, ubiquitous in marine phytoplankton, and may be involved in supplying OAA to the Tricarboxylic Acid (TCA) cycle to counter the drain of 2-oxoglutarate (also called a-ketogluterate) C skeletons to the NH_4^+ assimilation/amino acid biosynthesis pathway (Fig. 4, Guy et al. 1989, Vanlerberghe et al. 1990, Kroth et al. 2008). Because the TCA cycle generates electrons for the respiratory/mitochondrial electron transport chain, NH_4^+ assimilation has the potential of reducing this electron flow, and therefore ATP production, unless there is a source of OAA to the TCA cycle (Guy et al. 1989).

Appendix 2.3 Nitrogen assimilation

C and N assimilation are tightly linked because they share the flow of energy from light, and because fixed C provides skeletons for N assimilation. Additional energy for N reduction is supplied from respiration of fixed C (Fig. 3)

NH_4^+ is key to N assimilation and the first steps of amino acid biosynthesis because this is the only form of N that can be attached to oxogluterate (also known as a-ketogluterate), supplied by the TCA cycle, to produce the amino acid glutamate via the action of the enzymes glutamine synthetase (GS) and glutamate synthase (GOGAT). These reactions require input of reductant and ATP (Fig. 3). Multiple forms of the GS/GOGAT enzymes, localized both to the cytosol and to the chloroplast, exist in phytoplankton (i.e. Huppe and Turpin 1994). Recent genome sequencing efforts have demonstrated that in diatoms, the plastid-localized set is comprised of GSII and a ferredoxin-dependent form of GOGAT (Fd-GOGAT), thought to be responsible for the assimilation of NH_4^+ produced by NO_3^- reduction (Hockin et al. 2012). A second, GSIII and NADPH-dependent GOGAT set is localized outside the chloroplast and might assimilate NH_4^+ produced by cellular processes (Fig. 3), uptake and deamination of organic N sources (amino acids, purines etc) and direct NH_4^+ uptake (Mock et al. 2008, Brown et al. 2009, Hockin et al. 2012).

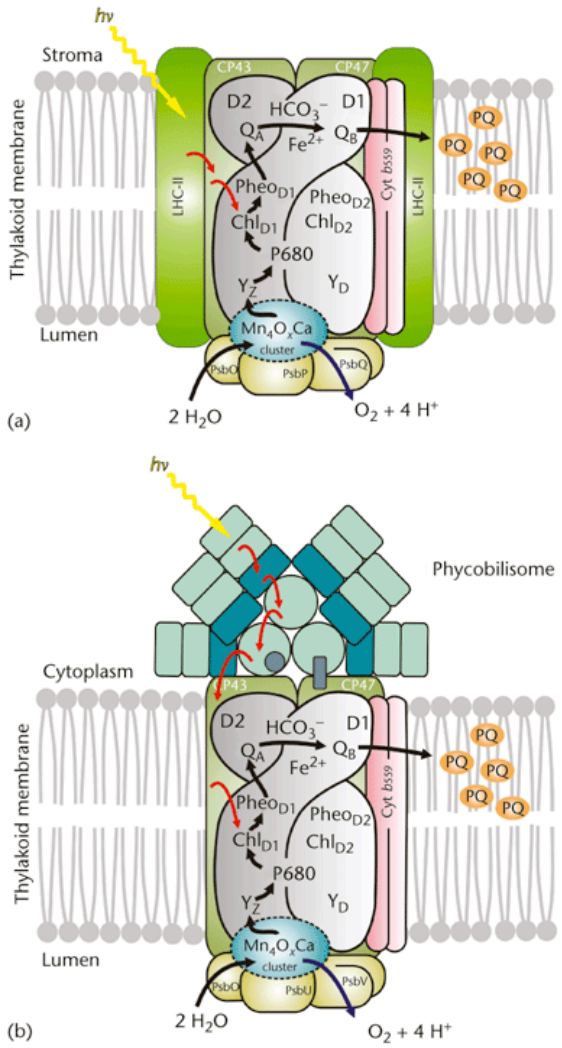

Figure A.2.1 Reproduced from Govindjee et al. 2010; PSII in a) eukaryotes and b) prokaryotes. The core of PSII is composed of the proteins D1 and D2 that bind P680, a pair of chlorophylls, and Chl_{D1}, the primary electron donor. Together, these chlorophylls make up the reaction center. CP43 and CP47 constitute the interior PSII antenna system (not to be confused with the peripheral LHCII and Phycobilisome antennae) and Mn4OxCa is the manganese cluster involved in splitting and removing electrons from water.

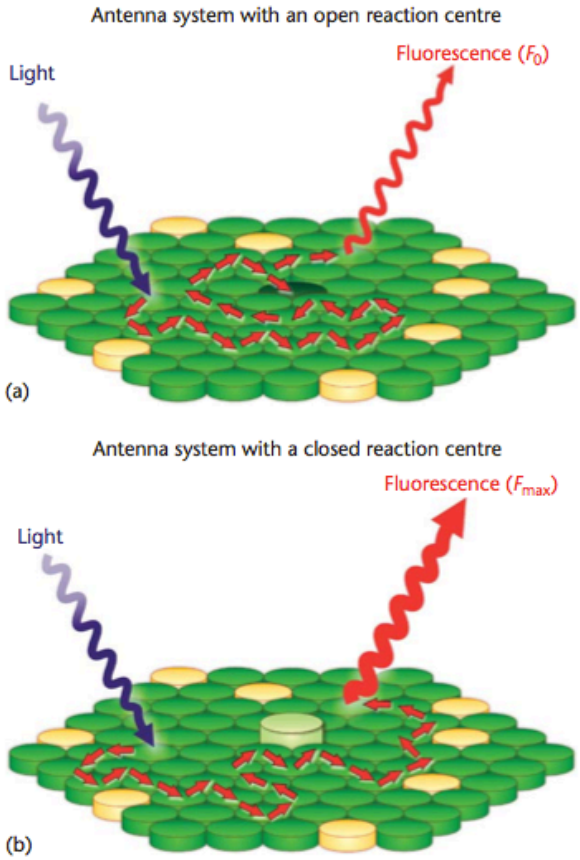

Figure A.2.2 Reproduced from Govindjee et al. 2010; Excitation energy transfer among Chl *a* and carotenoid molecules in a "generic" LHC II antanna (small red arrows). Green disks represent Chl *a* molecules and orange disks represent accessory pigment molecules. a) Energy transfer to an open reaction center with minimal fluorescence emission and b) energy transfer to a closed reaction center with maximal fluorescence emission

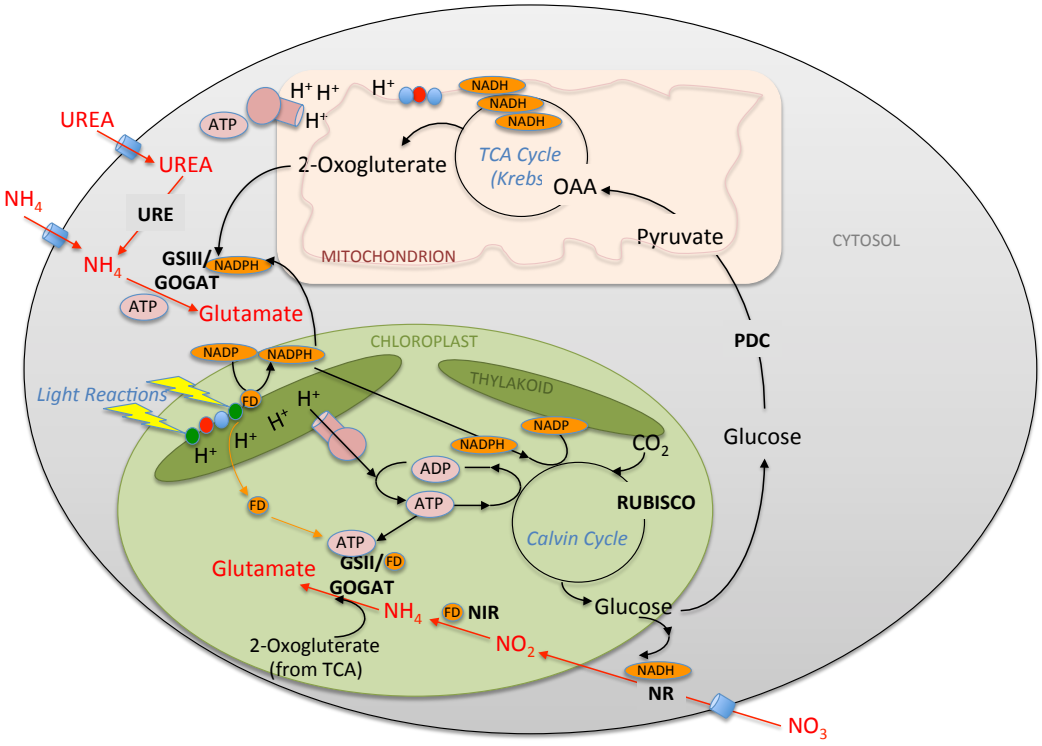

Figure A.2.3. Interactions between carbon metabolism (black lines) and nitrogen metabolism (red lines) in a photosynthetic cell. Electron carriers in orange, ATP in pink, ATP synthase enzyme in pink, FD=ferredoxin, NADPH=nicotinamide adenine dinucleotide phosphate, ATP=adenosine triphosphate, NR=nitrate reductase, NiR=nitrite reductase, GS/GOGAT=glutamine synthetase and glutamate synthase, URE=urease, PDC=pyruvate dehydrogenase complex, OAA=oxaloacetate, TCA=Tricarboxylic Acid Cycle, also known as the Krebs cycle. Green oval is chloroplast with thylakoid membranes, peach rectangle is mitochondrion and grey is cytosol of the cell. **Nitrate Reduction:** The first step, catalyzed by NR, reduces NO_3^- to nitrite (NO_2^-) by the addition of two electrons from NADH (most marine phytoplankton) or NADPH (green algae and terrestrial plants), and takes place in the cytosol. Subsequently, NO_2^- is transported into the chloroplast where it's reduced by NiR to NH_4^+ with six electrons donated from FD. **Ammonium assimilation/chloroplast:** NH_4 reduced from NO_3^- is subsequently combined with 2-oxogluterate via GSII/Fd-GOGAT requiring reductant from FD and ATP to produce glutamate. **Cytosol:** Glutamate is also synthesized from NH_4^+in the cytosol via GSIII/NADPH-GOGAT.

Appendix 5

Appendix 5.1 Sources of Knowledge

We would know nothing about the ecology of copepods in the San Francisco Estuary were it not for the foresight that led to the long-term IEP monitoring program, the high quality of the work done by that program, and the persistent support in the agencies for maintaining it. Nevertheless, most of our knowledge of copepod ecology more generally comes from laboratory experiments. These generally have one of two objectives: to determine what the organism can do, or to determine what it is actually doing in the estuary.

For the first objective, investigators may examine the sensory capability of the organism, its swimming, feeding, and mating behavior, its maximum growth or development rate, its metabolic and nutritional requirements, or its sensitivity to water quality. These sorts of experiments often use copepods obtained from cultures to remove the signal of past environmental variability and allow a focus on the animal's capabilities (e.g., Ger et al. 2010). Many species of copepod have been cultured in many different laboratories worldwide, and some of these cultures have been maintained for years. Typically cultures are fed a mixture of phytoplankton although, in some cases, single phytoplankton or microzooplankton species have proved to be adequate food for the entire life cycle of some species (Stoettrup et al. 1986).

For the second class of experiments, copepods are collected in the estuary and transported to the laboratory for setting up experiments. This is the approach used in most studies to determine feeding, growth, and development rates under environmentally realistic conditions (e.g., Kimmerer and McKinnon 1987, Bouley and Kimmerer 2006, Gifford et al. 2007).

Information from laboratory studies is often extended to field conditions using models of various processes or of population dynamics. For example, models can be used to examine development (Gentleman et al. 2008) or to estimate mortality rates from the distributions of life stages in the field, if their development times are known (Kimmerer and McKinnon 1987, Aksnes and Ohman 1996). Models have also been used to estimate how mechanisms for mate-searching affect the minimum population density from which a population of copepods can recover (Kiørboe 2007, Choi and Kimmerer 2008), and to examine the flow or chemical field around a swimming copepod (Bearon and Magar 2010, Jiang and Kiørboe 2011). Life-cycle models are rarer than models of individual processes, but recently individual-based models are coming into use for copepods (e.g., Dur et al. 2009), and we are preparing an IBM of *Pseudodiaptomus forbesi*.

Appendix 5.2. Notes on *Acartia* species and their relatives

The family Acartiidae includes two genera present in the SFE, *Acartia* and *Acartiella*. Species within subgenera of *Acartia* can be difficult to tell apart morphologically, and molecular evidence is mounting that cryptic speciation is ubiquitous within the subgenera *Acanthacartia* and *Acartiura* (McKinnon et al. 1992, Caudill and Bucklin 2004, Chen and Hare 2008). These subgenera are represented in the San Francisco Estuary by two and one species respectively. *A.* (*Acanthacartia*) *californiensis* is the only one whose name is correct. The species identified as *A.* (*Acanthacartia*) *tonsa* based on morphology is almost certainly a different species from the one so named from the east and Gulf coasts of North America and Europe (Caudill and Bucklin 2004). Copepods from the east and west coasts identified as *A.* (*Acartiura*) *clausi* were unable to interbreed (Carrillo et al. 1974). Painter (1966), Caskey (1976), and Ambler et al. (1985) referred to *A. clausi*, but the species in the SFE more closely resembles *A. hudsonica* (Bradford 1976). We have examined several specimens from the 1978-1981 samples, all of which match the description of *A. hudsonica* but not that of *A. clausi.* Collections from nearby Tomales Bay contained these species as well as *A. (Acartiura) omorii* (Kimmerer 1993), and it is possible that this species has occurred in SFE as well.

Ambler et al. (1985) reported a seasonal cycle in which *A.* "*clausi*" was very abundant in winter, and *A. californiensis* in summer, with total abundance of *Acartia* spp. rather constant throughout the year, while *A. tonsa* was uncommon. In contrast, samples taken in 1999-2002 showed *A. hudsonica* to be abundant throughout the year, with *A. californiensis* and *A. tonsa* also present all year and abundant at times (Kimmerer et al. 2005). Unfortunately the IEP monitoring program does not distinguish among the species present or sample their entire habitat, so there is no way now to determine when this change happened or why.

Acartiella superficially resembles *Acartia*, but is actually a very different organism. It is most abundant in the LSZ in late summer to fall and rare at other times and places (Fig. 3). Morphologically it is obviously a predator based on the shape of its mouthparts (Tranter and Abraham 1971), and its long antennae suggest a capability to detect rather large organisms from a distance. Nothing is published on its ecology, but experiments show that it consumes other copepods (York et al. in revision).

Appendix 6

Appendix 6.1: Additional Figures

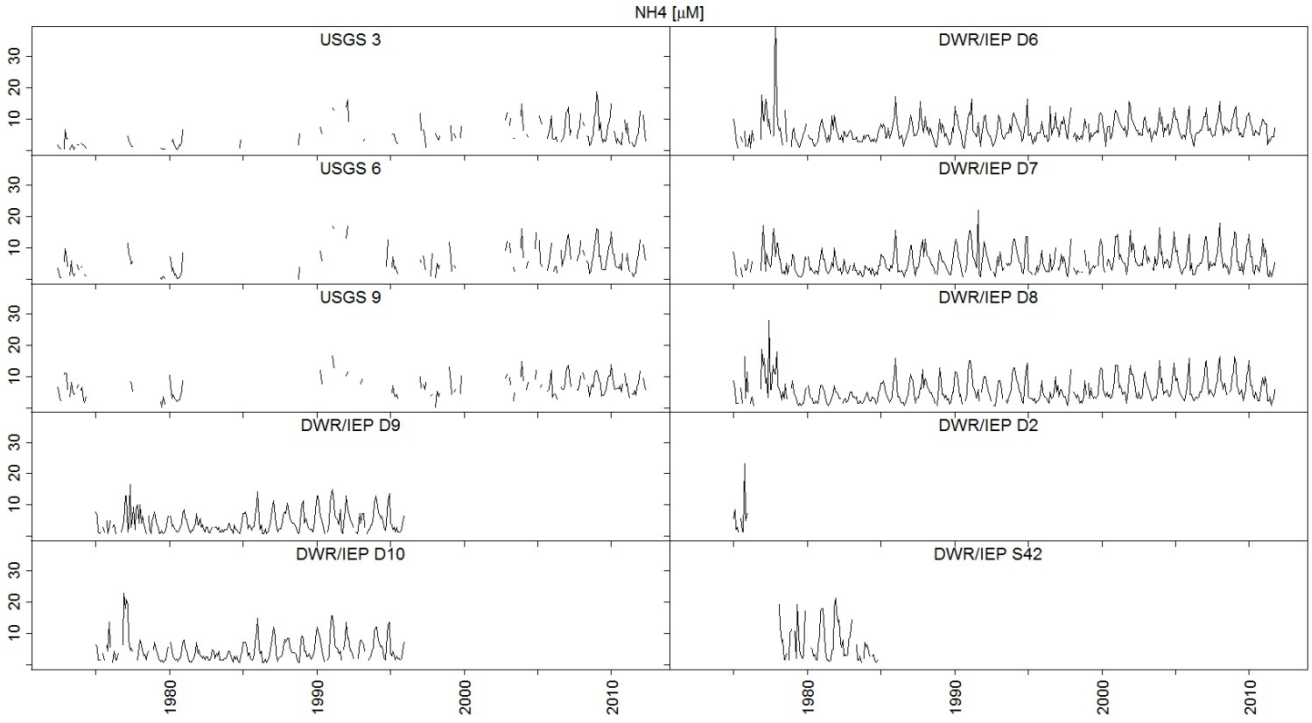

Fig A.6.1.1 Available NH4 data for all DWR/IEP [1] and USGS[2] stations in Suisun Bay. DWR/IEP stations D6, D7 and D8 have the most complete record and are presented in greater detail in Figure 6.1.

[1]http://www.water.ca.gov/bdma/meta/Discrete/data.cfm

[2]http://sfbay.wr.usgs.gov/access/wqdata/

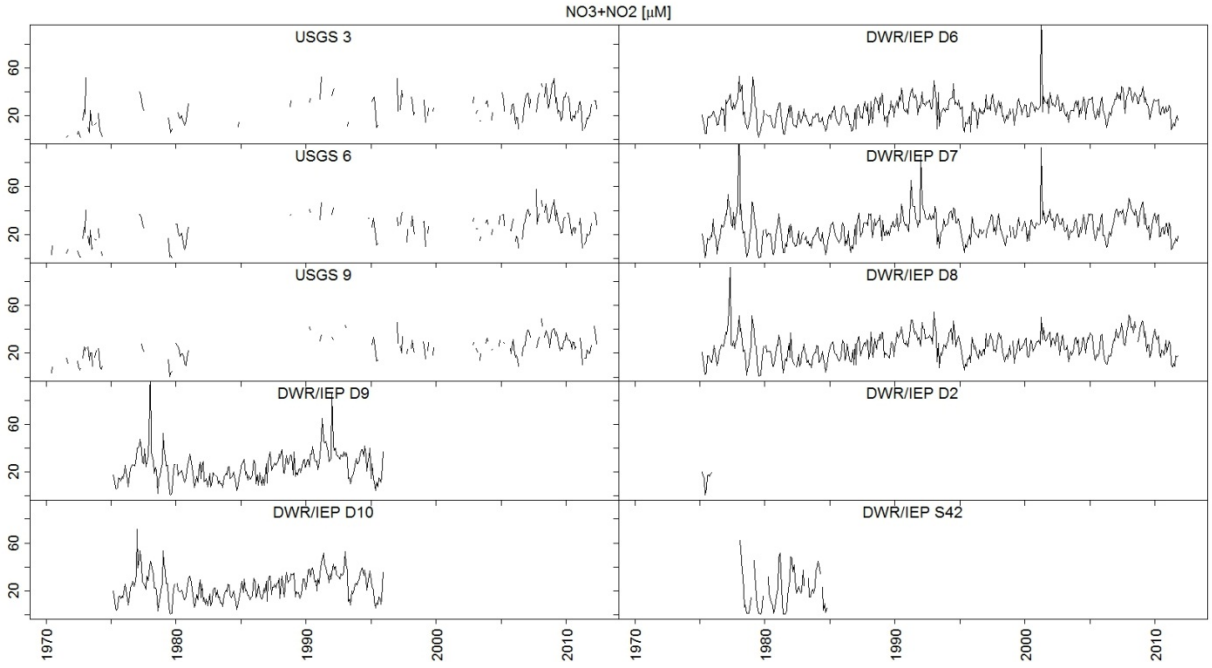

Fig A.6.1.2 Available NO3+NO2 data for all DWR/IEP and USGS stations in Suisun Bay

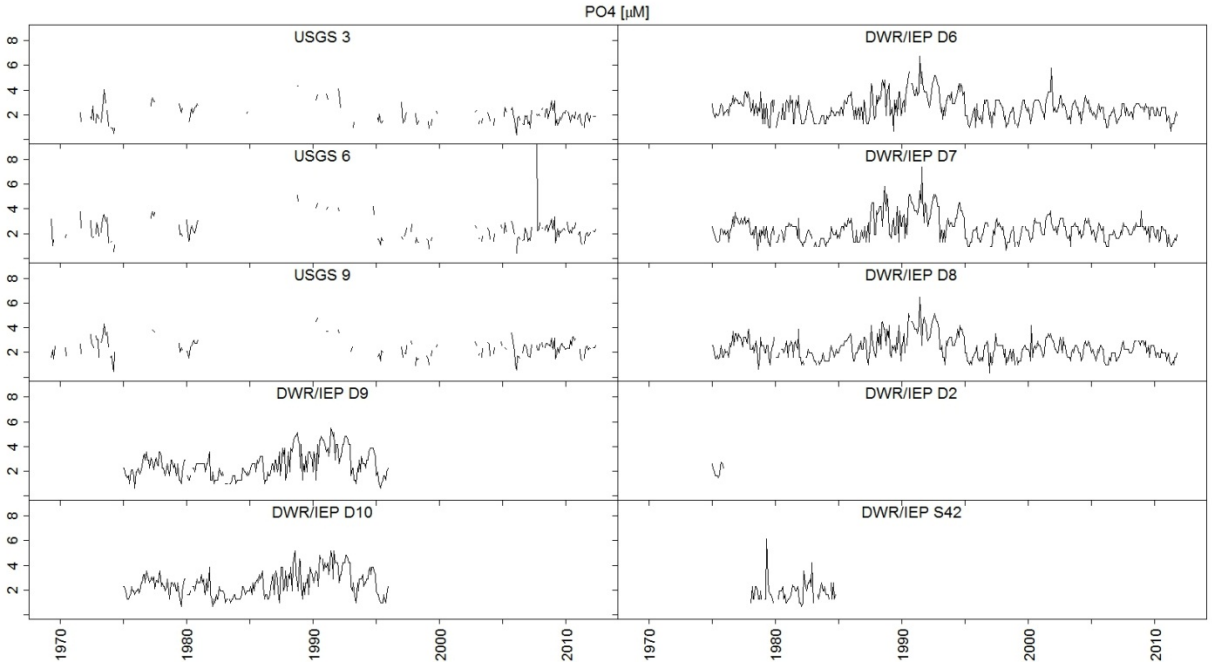

Fig A.6.1.3 Available PO4 data for all DWR/IEP and USGS stations in Suisun Bay

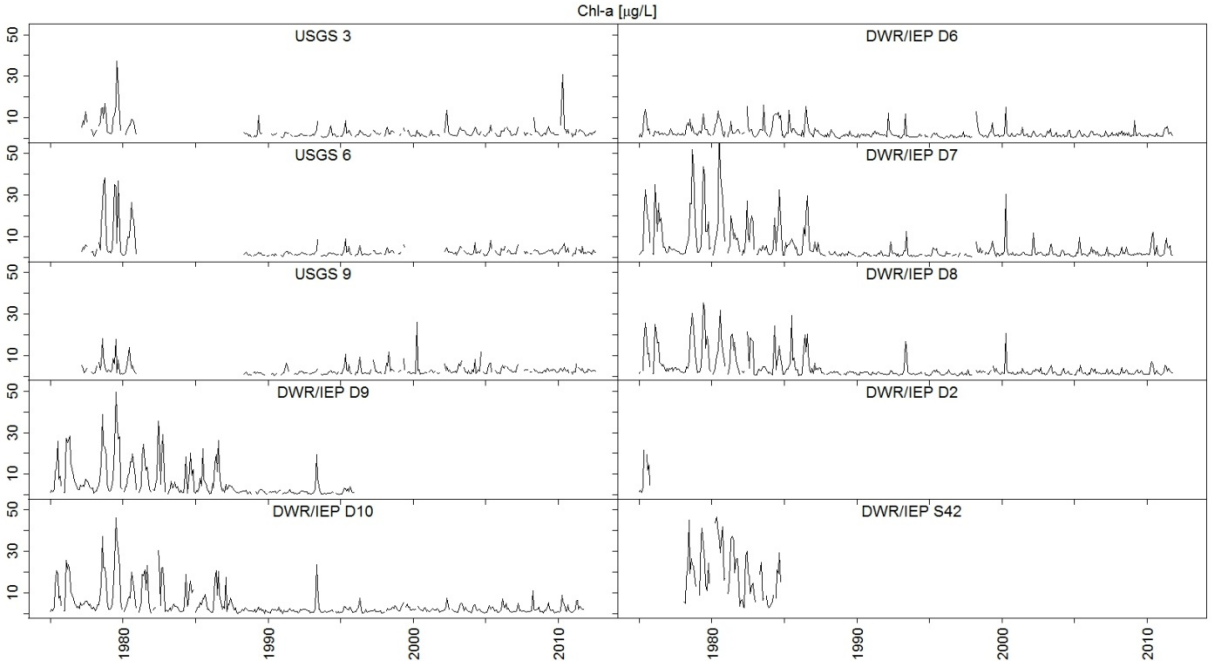

Fig A.6.1.4 Available chlorophyll-*a* data for all DWR/IEP and USGS stations in Suisun Bay

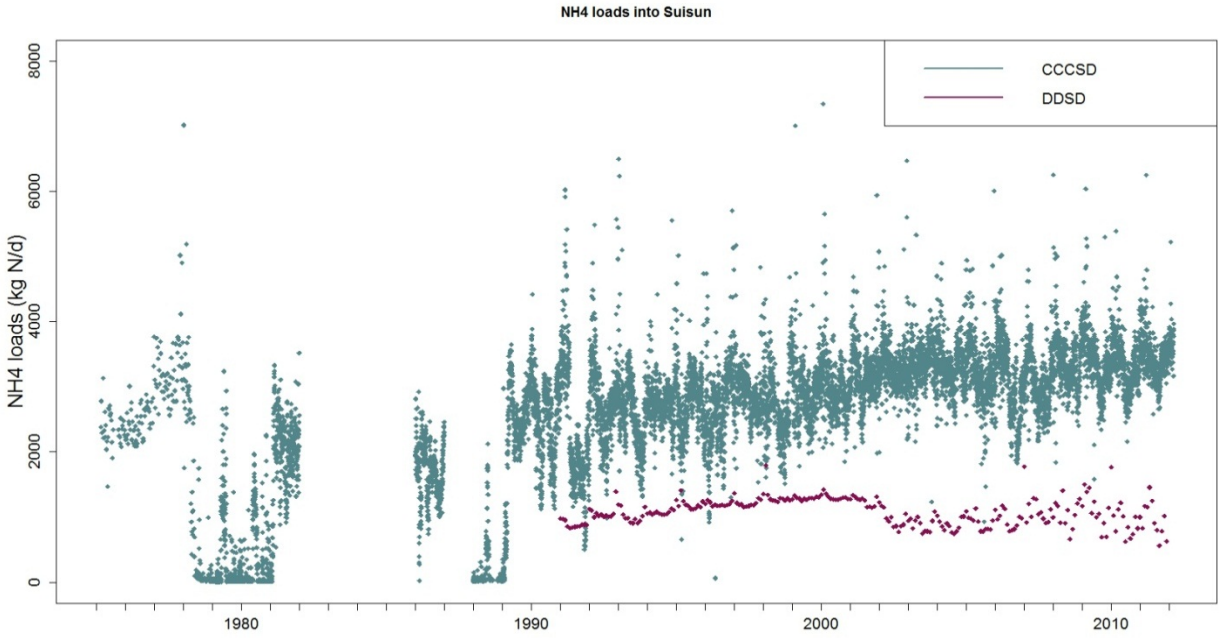

316 **Fig A.6.1.5** Effluent NH4 loads from the two major NH4 dischargers to Suisun Bay, CCCSD and DDSD, including trial periods of nitrification at
317 CCCSD (1977-1982, 1987-1988) Nitrification processes at FSSD reduce NH4 loads to approximately 1% of the other two dischargers and are therefore not included here.

318

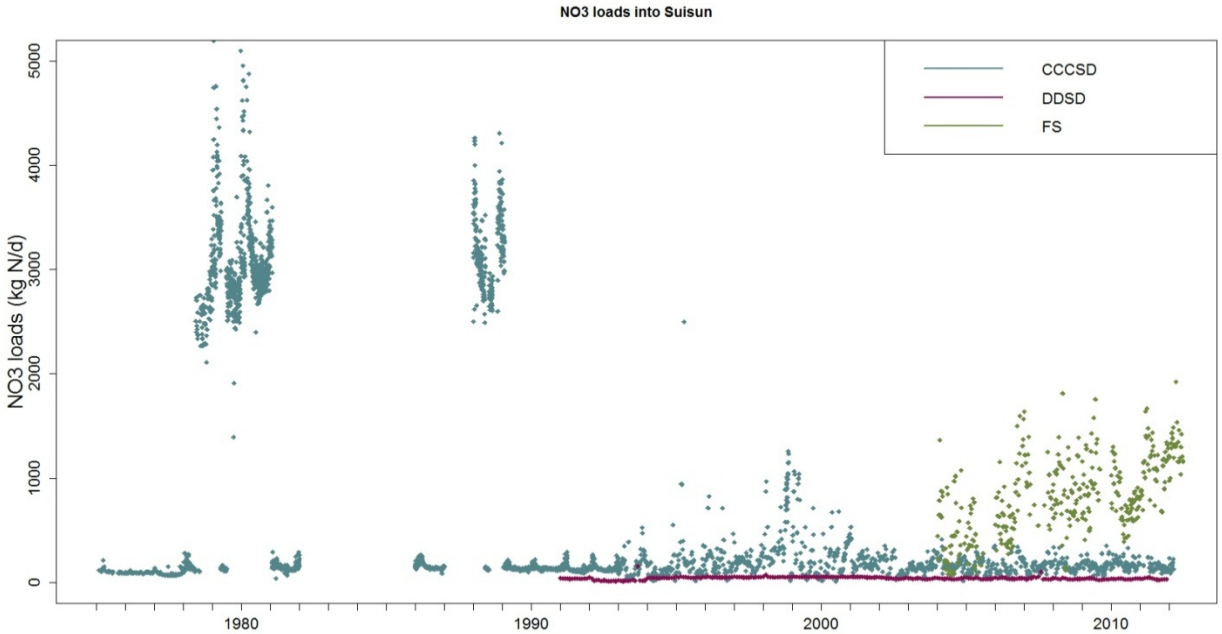

319 **Fig A.6.1.6** Effluent NO3 loads from the three major NH4 dischargers to Suisun Bay, FSSD, CCCSD, and DDSD, including trial periods of
nitrification at CCCSD (1977-1982, 1987-1988). Nitrification processes at FSSD increase NO3 loads to well above those at either CCCSD or
320 DDSD.

321

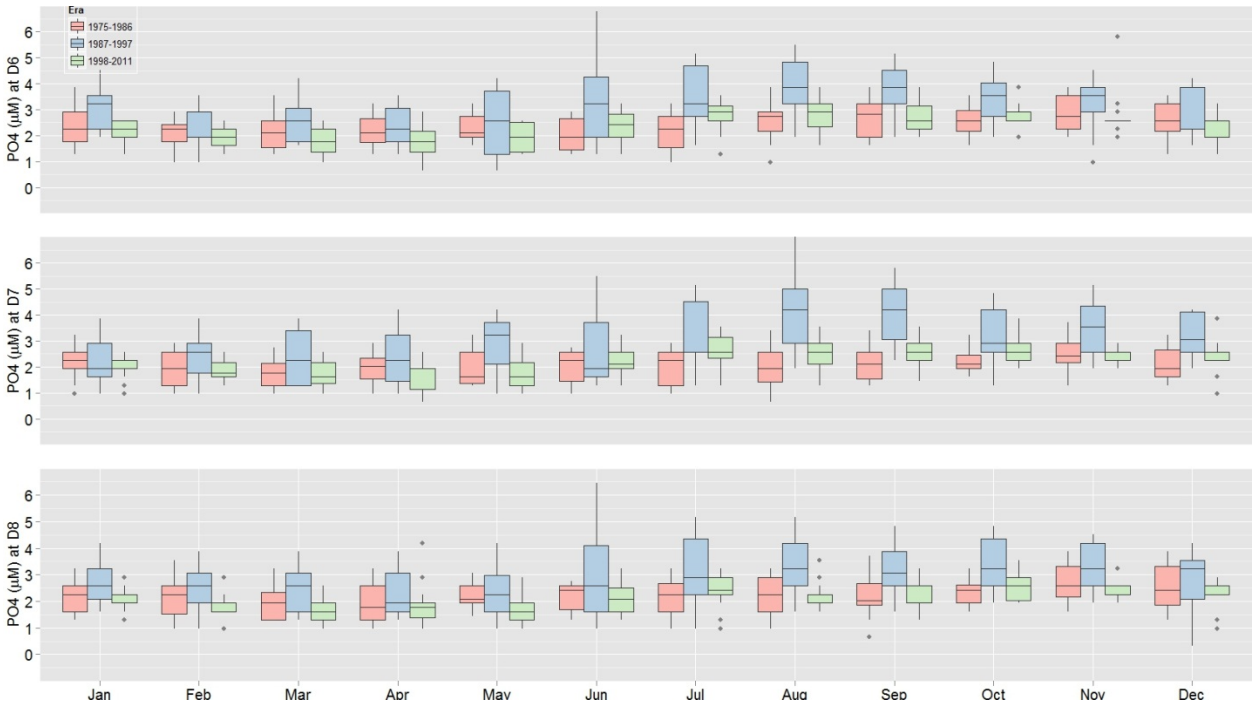

322

323 **Fig A.6.1.7** PO4 data at DWR/IEP stations D6, D7 and D8. Data were first aggregated into three eras (1975-1986, 1987-1997 and 1998-2011), and then averaged by month within each era

324

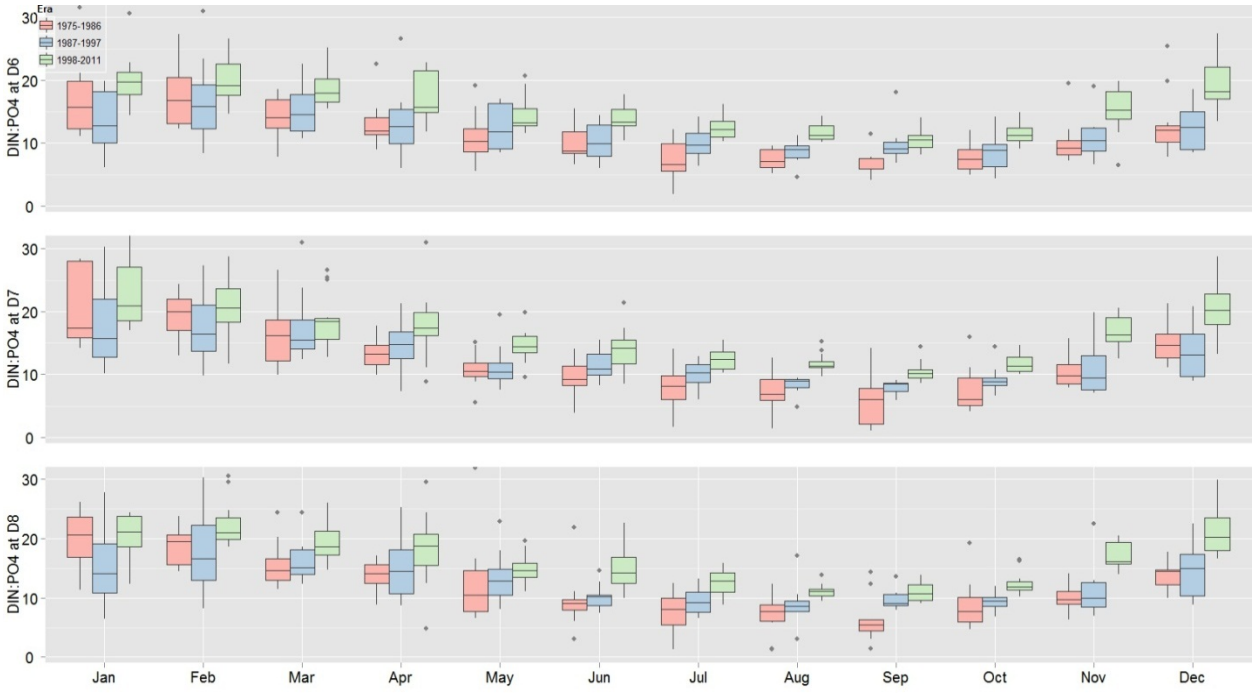

325

326 **Fig A.6.1.8** Ratio of DIN (NO3+NO2+NH4) to PO4 at DWR/IEP stations D6, D7 and D8. Data were first aggregated into three eras (1975-1986, 1987-1997 and 1998-2011), and then averaged by month within each era

327

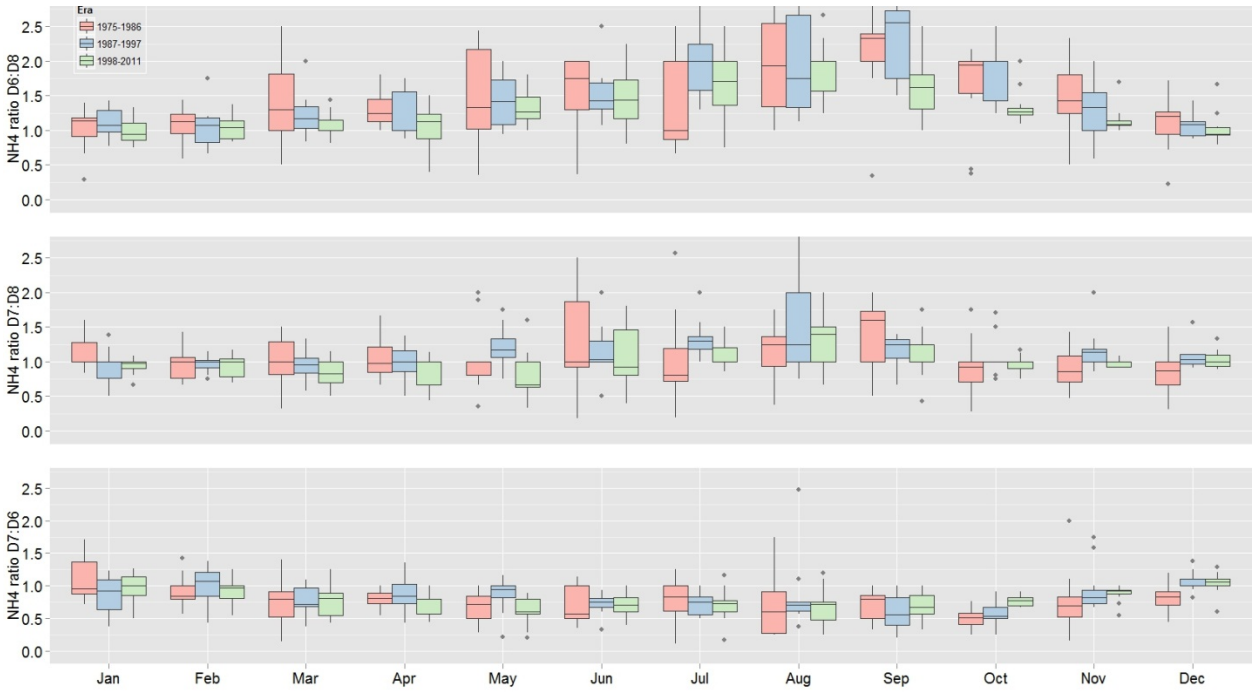

Fig A.6.1.9 Ratio of NH4 between each of the three key stations in Suisun Bay. This analysis will indicate spatial variability of NH4 concentrations i Suisun Bay. Data were first aggregated into three eras (1975-1986, 1987-1997 and 1998-2011), and then averaged by month within each era

Fig A.6.1.10 Ratio of NO3+NO2 between each of the three key stations in Suisun Bay. This analysis will indicate spatial variability of NO3 concentrations in Suisun Bay. Data were first aggregated into three eras (1975-1986, 1987-1997 and 1998-2011), and then averaged by month within each era

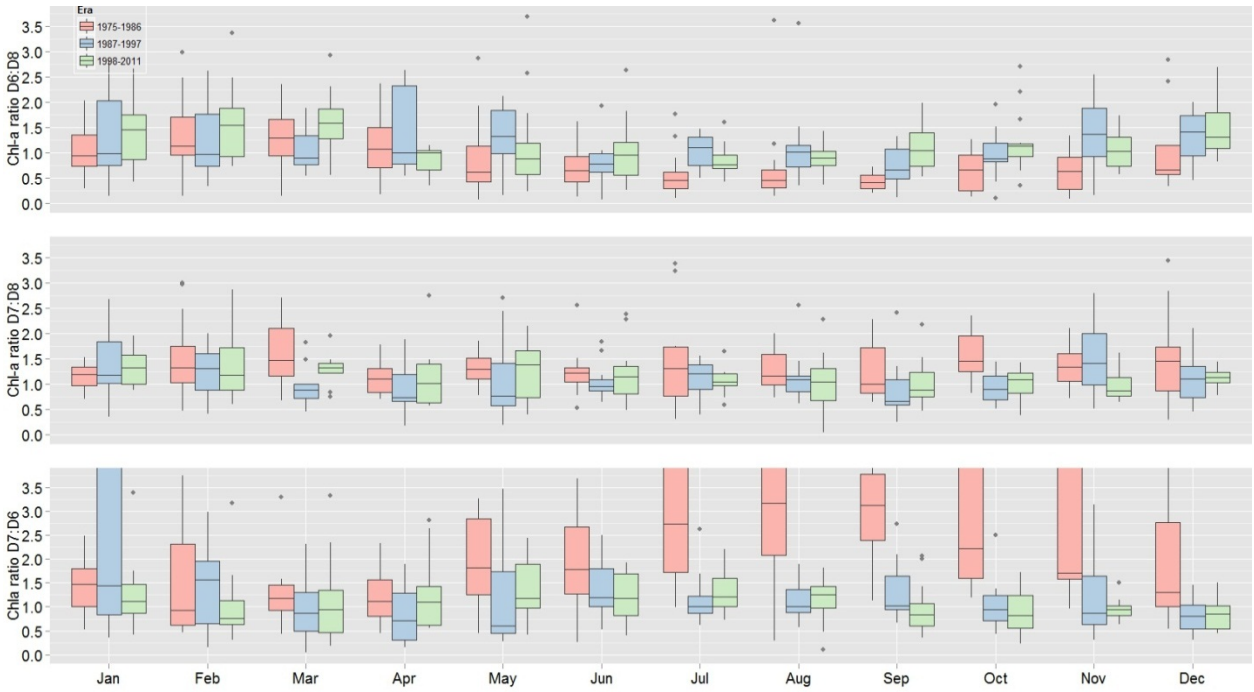

Fig A.6.1.11 Ratio of Chl-a between each of the three key stations in Suisun Bay. This analysis will indicate spatial variability of chl-*a* concentrations in Suisun Bay. Abrupt changes in chlorophyll-*a* concentrations brought about by the invasion of the *Corbula amurensis* clam is reflected in this figure. Data were first aggregated into three eras (1975-1986, 1987-1997 and 1998-2011), and then averaged by month within each era

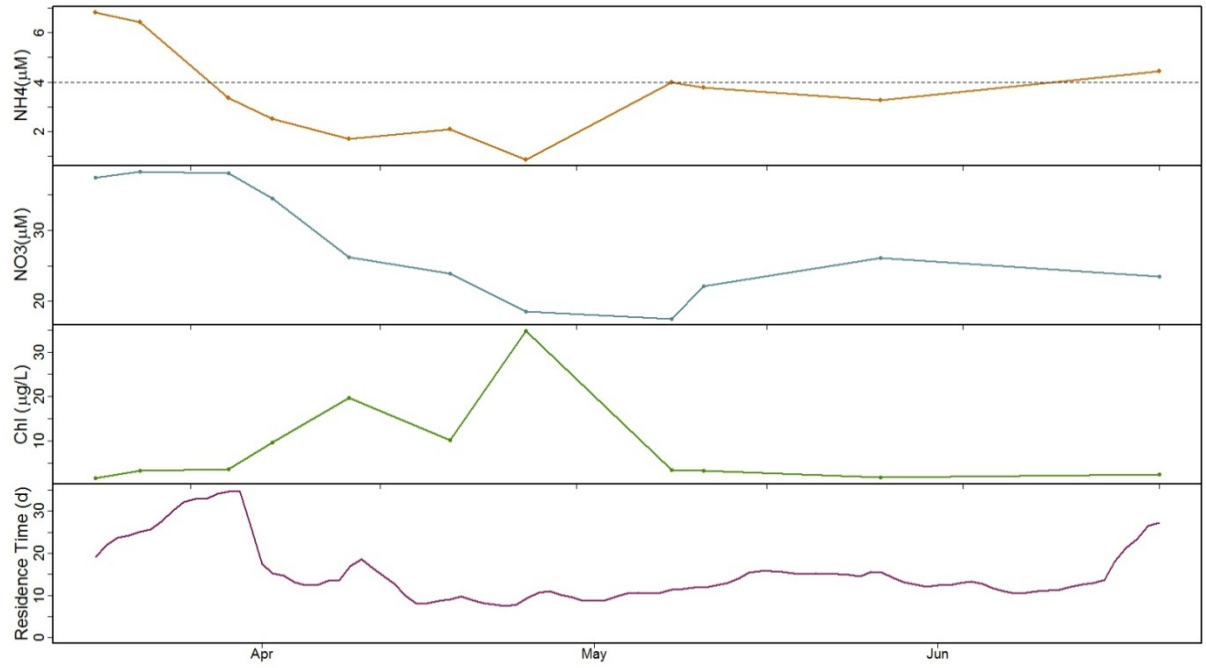

Fig A.6.1.12 Time series of NH4, NO3 and chlorophyll-a data collected by SFSU-RTC near DWR/IEP station D7 on 11 dates during Spring and Summer 2010 in Suisun Bay. The dashed line in panel a is at 4µM, the concentration believed to inhibit NO3 uptake and limit primary production (Dugdale et. al, 2007).. Residence time was calculated by dividing the volume of Suisun Bay (6.54e11 L) by daily advective flows

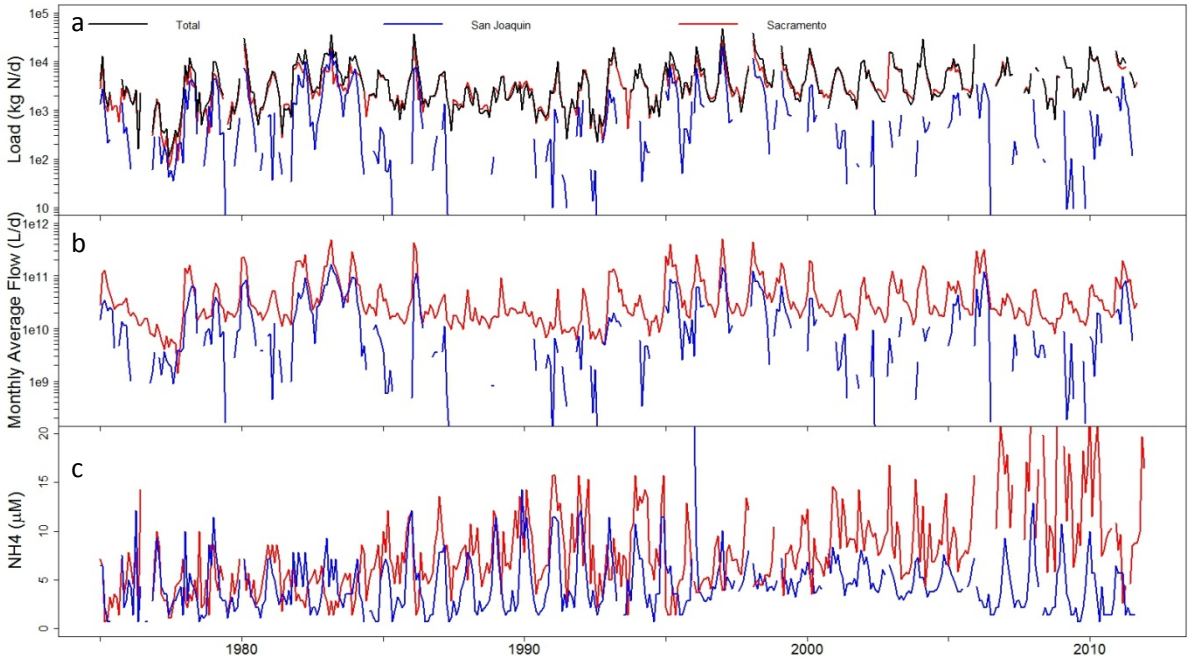

Fig A.6.1.13 Estimates of Delta efflux NH4 loads into Suisun Bay (panel a), Delta flow through Suisun Bay (panel b) and concentrations measured in the Sacramento and San Joaquin Rivers just prior to entering the Delta. Contributions from the Sacramento River are shown in red, and those from the San Joaquin River are shown in blue. Loads are dominated by the Sacramento River (panel a), which includes effluent from Sacramento Regiona Water Treatment Plant. Calculations were performed in a similar manner to those used by Jassby and Cloern (2000) to estimate organic matter loads to Suisun Bay. Details of calculations of these loads can be found in Appendix 6.2.

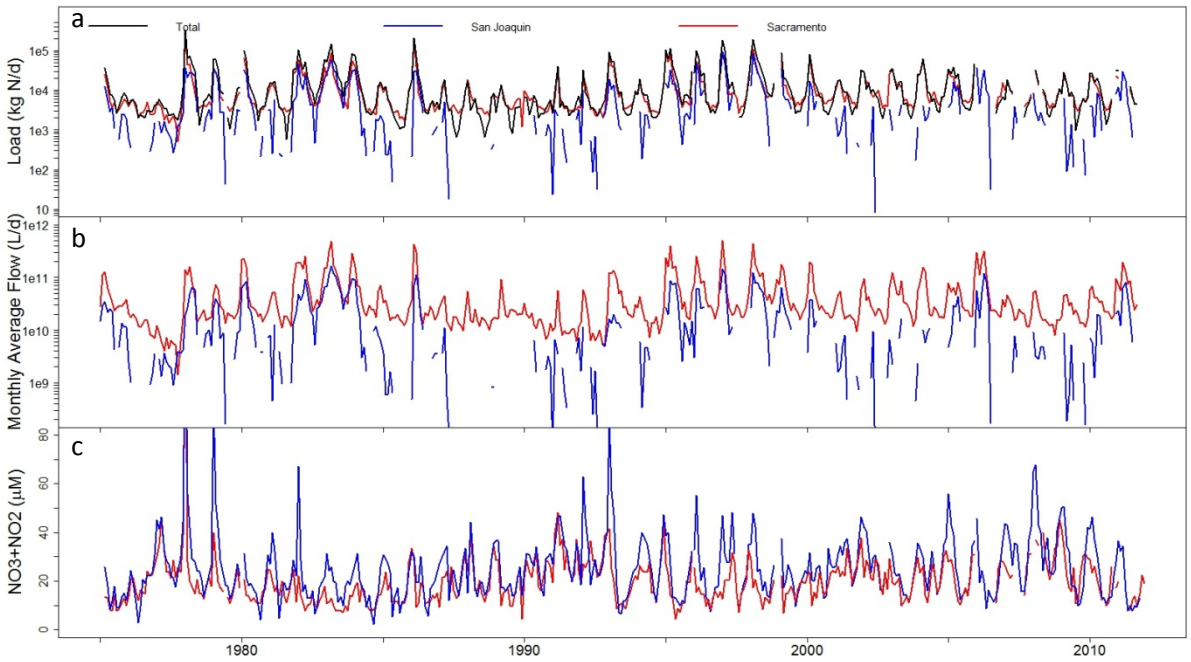

Fig A.6.1.14 Estimates of Delta efflux NO3+NO2 loads into Suisun Bay (panel a), Delta flow through Suisun Bay (panel b) and concentrations measured in the Sacramento and San Joaquin Rivers just prior to entering the Delta. Contributions from the Sacramento River are shown in red, and those from the San Joaquin River are shown in blue. Despite higher concentrations in the San Joaquin River (panel c), substantially higher flow in the Sacramento River (panel b) causes Sacramento loads to be dominant (panel a). Calculations were performed in a similar manner to those used by Jassby and Cloern (2000) to estimate organic matter loads to Suisun Bay. Details of calculations of these loads can be found in Appendix 6.2.

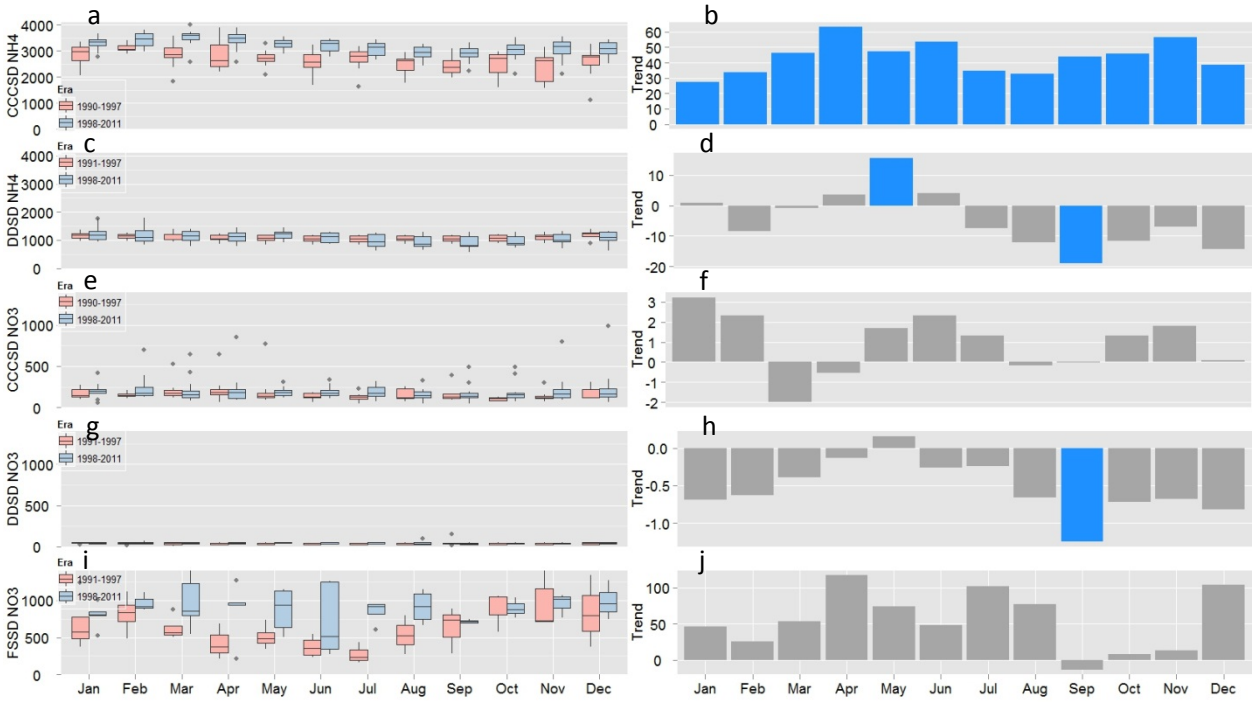

Fig A.6.1.15 Seasonal and long-term variability in effluent NH4 and NO3 loads from the three major dischargers to Suisun Bay, CCCSD, DDSD and FSSD, after trial periods of nitrification at CCCSD (1977-1982, 1987-1988). Data was a combination of self-reported effluent flow and either actual measured concentrations, or approximate effluent concentrations from the literature (see section 6.2.2 for further detais). Nitrification processes at FSSD reduce NH4 loads to approximately 1% of the other two dischargers and are therefore not included here. Loads (kg N d^{-1}) were first aggregated into two eras (which varied based on data availability of the individual discharger), and then averaged by month within each era (panels a,c,e,g, and i). Long-term trends were characterized by the Theil slope (kg d^{-1} y^{-1}) (see description in Section 6.2.3) (panels b,d,f,h and j). Blue bars indicate statistically significant trends with $p<0.05$ as determined by the Kendall Tau test.

Appendix 6.2: Estimating Delta Efflux Loads

The approach for calculating nutrient loads from the Delta into Suisun Bay was adapted from an approach used by Jassby and Cloern (2000). We quantified loads past Rio Vista (representing flow originating in the Sacramento River, Q_{rio}) and loads past Twitchell Island (representing flow originating in the San Joaquin River, Q_{west}), and combined these to estimate total load on a monthly average basis

$$Load = Q_{west}C_{west} + Q_{rio}C_{rio}$$

Flow:

Flow values were taken from DWR DAYFLOW records. Both Q_{west} and Q_{rio} are calculated values, using actual measured flows at gages throughout the Delta. Flow values were available daily, and we took a monthly average to calculate monthly average loads.

Q_{west}:

$Q_{WEST} = Q_{SJR} + C_{SMR} + Q_{MOKE} + Q_{MISC} + Q_{XGEO} - Q_{EXPORTS} - Q_{MISDV} - 0.65\ (Q_{GCD} - Q_{PREC})$

Q_{rio}:

$Q_{RIO} = Q_{SAC} + Q_{YOLO} - Q_{XGEO} - 0.28\ (Q_{GCD} - Q_{PREC})$

Concentration:

DWR/IEP and USGS conduct monthly water quality monitoring in the Delta, and we combined these concentrations with monthly-averaged flow to produce monthly-averaged estimates of load. Stations used for C_{west} and C_{rio} varied throughout the period of 1975-2011 because of changes in station operation (Table A.2.1). Between 1975 and 1975, DWR/IEP station D24 was used for C_{rio} and DWR/IEP station D16 was used to represent for C_{west}. Unfortunately, monitoring at both of these stations ceased in 1995, and we were forced to substitute using stations whose monitoring continued past 1995. We performed multivariate linear regressions of D24 and D16 data from 1975-1995 against data from nearby stations from the same period in order to develop the substitutions that would be used post-1995. Starting in 2006, we made single-station substitutions for both C_{west} and C_{rio}. At this time, nutrient monitoring intensified at DWR/IEP station D19 and began at USGS station 657, which is nearly collocated with DWR/IEP D24. Details on stations substitutions can be found in the table below. Locations of stations relative to Q_{west} and $Q_{rio,}$ as well as relative to each other, can be found in Figure A.2.2

Uncertainty:

Although the method used to estimate Delta efflux loads was the same as was previous used by Jassby and Cloern (2000) to estimate organic matter loads to Suisun Bay, there is some uncertainty associated with the constituent data sets used in this calculation. Q_{west} and Q_{rio} are both calculated values, not directly measured by flow gages. Although the formula used to calculate these terms is frequently reviewed and revised by DWR (as recently as 2012), a calculated value will never be as accurate as one that is measured. The DWR/IEP and USGS stations used are not continuous over the entire period 1975-2011. There are stations with continuous data from 1975-1995 (D16 and D24), which are also nearly collocated with DAYFLOW locations of Q_{west} and Q_{rio}, however both of these stations were dropped in 1995. A USGS station (657) that is nearly identical to the location of station D24 began monitoring for nutrients in 2006, but there were gaps in the record from 1995-2006 (at the former station D24) and from 1995-2011 (at the former station D19). Multivariate linear regressions from nearby stations filled these gaps with varying levels of accuracy (see r^2 values in Table A.6.2.1), but this station substitution introduces additional uncertainty into these estimates. In spite of these data gaps, the estimates made here are believed to be reliable as order of magnitude approximations and further modeling efforts in the Delta could help refine these estimates further.

References:

Jassby, A.D., and Cloern, J.E. (2000) Organic matter sources and rehabilitation of the Sacramento-San Joaquin Delta (California, USA). Aquatic Conservation: Marine and Freshwater Ecosystems 10: 323–352.

Tables and Figures:

		C_{west}	C_{rio}
1975-1995	NH4	D16[1]	D24[1]
	NO3+NO2	D16[1]	D24[1]
1996-2005	NH4	$0.311 * D26 + 0.235 * D28A + 0.320 * D4 - 0.001$ $r^2 = 0.77$	$0.165 * C3 + 0.551 * D4 + 0.022$ $r^2 = 0.52$
	NO3+NO2	$0.5305 * D26 + 0.1613 * D28A + 0.3812 * D4 - 0.020$ $r^2 = 0.93$	$0.200 * C3 + 0.809 * D4 - 0.023$ $r^2 = 0.85$
2006-2011	NH4	D19 $r^2 = 0.81$	USGS 657[2]
	NO3+NO2	D19 $r^2 = 0.84$	USGS 657[2]

Table A.6.2.1 DWR/IEP and USGS water quality monitoring stations used in combination with DWR DAYFLOW values Q_{west} and Q_{rio} to approximate Delta loads. After 1995, when both station D24 and D16 were dropped, there were gaps in the record that were filled by multivariate linear regression from nearby stations whose monitoring continued past 1995 (the resulting linear equation and r^2 values are shown here).
[1]Stations used by Jassby and Cloern (2000)
[2]Regression against D24 not possible because data from these two stations never coexisted

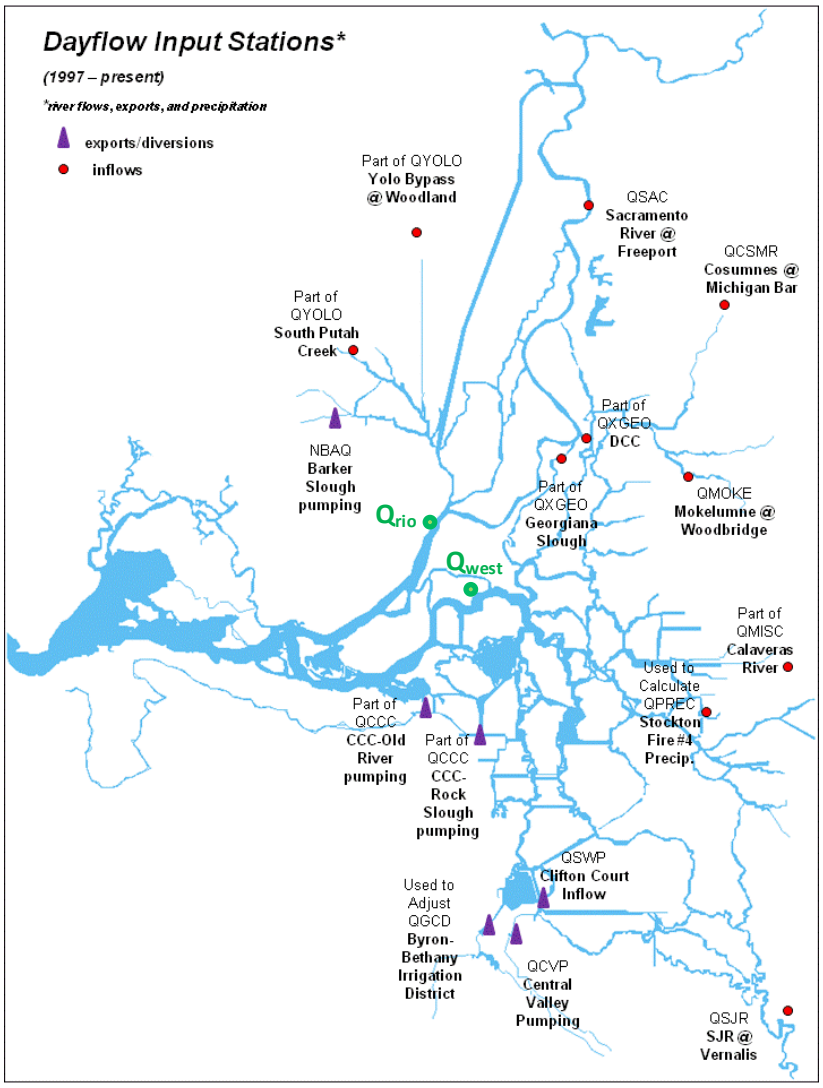

Figure A.6.2.1 Location DWR DAYFLOW gages (indicated by purple triangles). The values used in our estimation, Q_{west} and Q_{rio}, are calculated according to the following formulas and give approximation of flow past the points indicated above.

$Q_{WEST} = Q_{SJR} + C_{SMR} + Q_{MOKE} + Q_{MISC} + Q_{XGEO} - Q_{EXPORTS} - Q_{MISDV} - 0.65\ (Q_{GCD} - Q_{PREC})$

$Q_{RIO} = Q_{SAC} + Q_{YOLO} - Q_{XGEO} - 0.28\ (Q_{GCD} - Q_{PREC})$

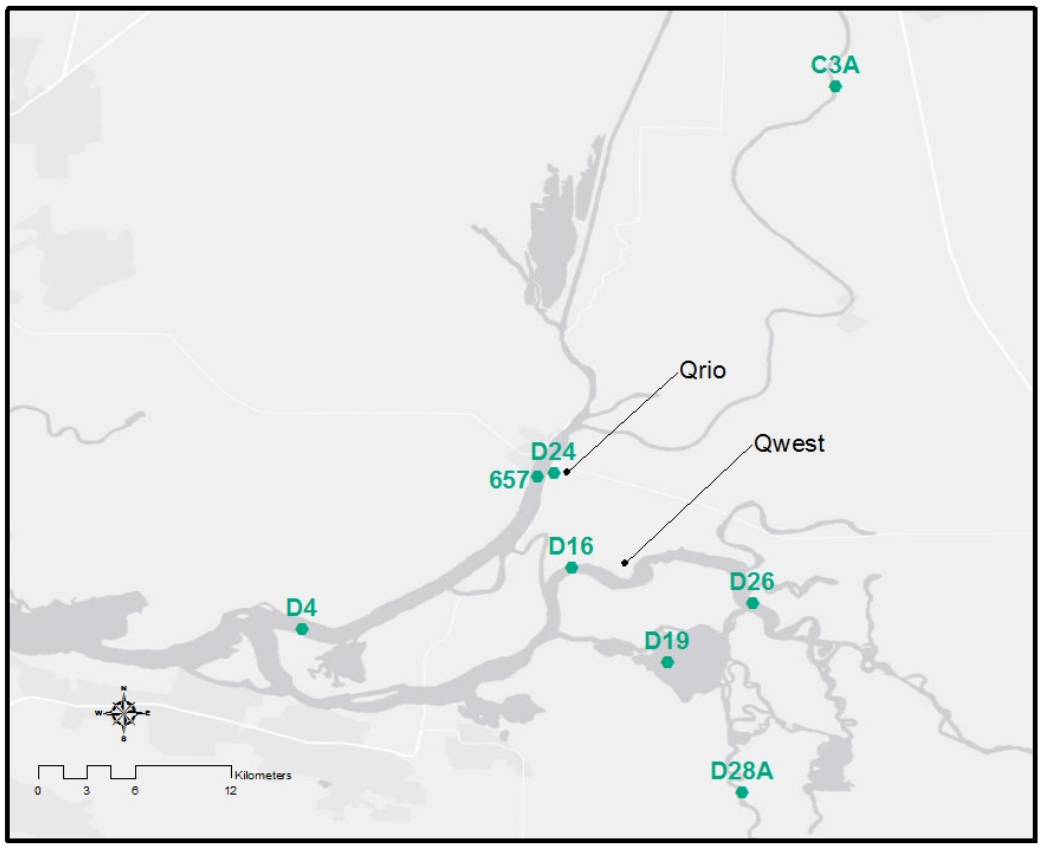

Figure A.6.2.2 Location of DWR/IEP and USGS water quality stations used in Delta loads estimate, as well as location of flow estimates.

Appendix 6.3: Estimating Stormwater Loads

Our approach to calculating stormwater loads is the following:

$$Load = P * RC * A * C$$

where

P = precipitation
RC = runoff coefficient
A = area of watershed
C = concentration of NH4 or NO3

Precipitation:

We used monthly values of precipitation for the entire Bay Area averaged over the period 1914-2005 (available from the Western Regional Climate Center) (Table 6.3.1).

Runoff Coefficients:

We calculated a single weighted-average runoff coefficient for each of the two watersheds that drain into Suisun Bay (Figure A.6.3.1). We calculated the % of each watershed in each land-use bin (agriculture, commercial, industrial, open, residential, transportation and water; Figure A.3.1) and then multiplied by a land-use specific runoff coefficient (Lent and McKee, 2011; Table A.6.3.2) in the following way:

$$RC = \%_{agr}RC_{agr} + \%_{comm}RC_{comm} + \%_{ind}RC_{ind} + \cdots$$

We used a low and high estimate of runoff coefficients bound the uncertainty of our estimates.

Area:

Concord watershed had a total area of 654 km^2, and Fairfield watershed had a total area of 867 km^2.

Concentration:

In 2010, 8 Bay Area watersheds were monitored for nutrients in both the wet season and the dry season (McKee and Gluchowski, 2011). We used the average of these different sites as our representative concentrations in our calculations (Table A.6.3.3)

References:

Lent, M.A. and McKee, L.J., 2011. Development of regional contaminant load estimates for San Francisco Bay Area tributaries based on annual scale Rainfall-Runoff and Volume-

McKee, L.J., and Gluchowski, D.C, 2011. Improved nutrient load estimates for wastewater, stormwater and atmospheric deposition to South San Francisco Bay (South of the Bay Bridge). A Watershed Program report prepared for the Bay Area Clean Water Agencies (BACWA). San Francisco Estuary Institute, Oakland CA.

Tables and Figures:

Jan	Feb	Mar	Apr	May	Jun	Jul	Aug	Sep	Oct	Nov	Dec
0.112	0.096	0.071	0.035	0.001	0.003	0.001	0.001	0.006	0.026	0.066	0.104

Table A.6.3.1 Average monthly precipitation values used to estimate stormwater runoff loads, in meters (available from the Western Regional Climate Center)

Land Use Type	Lower-Bound Runoff Coefficient	Upper-Bound Runoff Coefficient	Concord % Land Use	Fairfield % Land Use
Water	0	0	1.2%	4.7%
Open	0.09	0.34	53%	51%
Residential	0.2	0.39	26%	6.6%
Industrial	0.5	0.6	4.5%	1.6%
Commercial	0.5	0.6	6.3%	1.6%
Transportation	0.78	0.83	8.7%	5.5%
Agriculture	0.12	0.46	0.3%	29%
Weighted-average Runoff Coefficient:			**Concord low:** 0.22 **Concord high:** 0.42	**Fairfield low:** 0.15 **Fairfield high:** 0.40

Table A.6.3.2 Land-use specific run-off coefficients (Lent and McKee, 2011) were used in combination with % landuse in each Suisun Bay watershed to estimate an upper- and lower-bound runoff coefficient for the entire watershed

	Average wet season (Oct-Apr)	Average dry season (May-Sep)
NH4	0.332 mg/L	0.254 mg/L
NO3	1.01 mg/L	0.95 mg/L

Table A.6.3.3 Wet and dry season concentrations of NH4 and NO3 in stormwater (measured in 8 Bay Are watersheds in 2011, McKee and Gluchowski 2011).

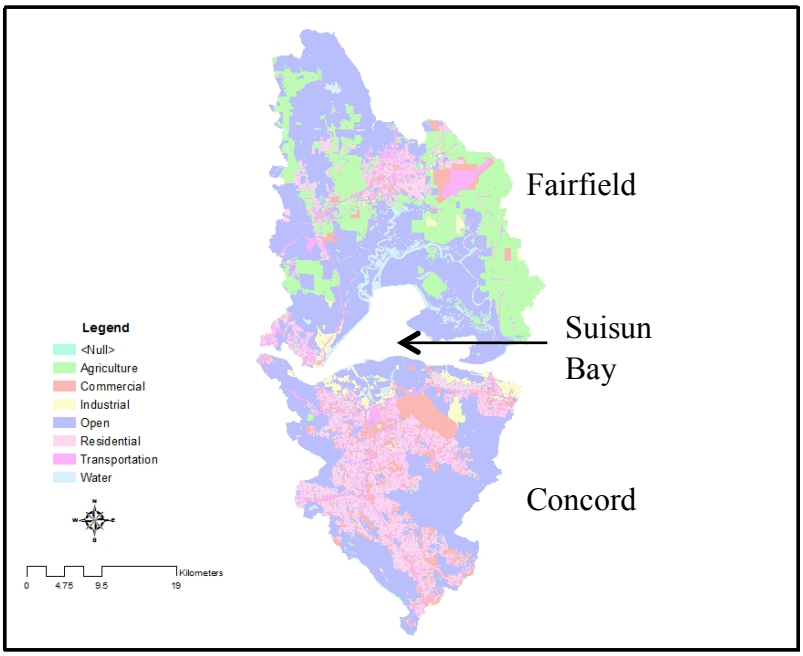

Figure A.6.3.1 Land-use breakdown for two watersheds that drain in Suisun Bay: Fairfield (north) and Concord (south)

Appendix 6.4: 1-box model for Suisun Bay

In order to evaluate the role of Suisun Bay in transforming incoming NH4 loads, we performed a 1-box mass balance using a well-mixed Suisun Bay as the control volume. We first performed a salinity balance in order to quantify tidal flows, and then performed a NH4 balance to evaluate the residual transformation/loss term. Data analysis with the box model focused on 2006-2011, when data from all load sources was most certain, and also on the months April-October, when residence time in Suisun Bay tends to be longest and when phytoplankton blooms have been historically observed. For these months, we assumed steady-state. Evaluation of assumptions is included in the description of each model.

Estimates of loads in and our were made using advective flow estimates from DWR DAYFLOW, tidal flow estimates from the salinity balance performed below, and concentration measurements from DWR/IEP and USGS monitoring stations. DAYFLOW measurements were extracted for the exact dates of DWR/IEP concentration measurements. The location of the flow and concentrations monitoring stations is shown in Figure A.6.4.1

Salinity Balance

To simplify our 1-box model, we made the following assumptions:

1. Treated Suisun as a well-mixed control volume
2. Steady state
3. Tidal dispersion on upstream side (exchange with D19, 657) considered negligible

The terms used in our mass balance were the following, and we solved for Q_{tide}:

1. S_{river} = flow-weighted average of S_{D19} and S_{657}
2. S_{su} = average(S_{D6}, S_{D7}, S_{D8})
3. $S_{sp} = S_{D41}$
4. $Q_{adv} = Q_{west} + Q_{rio}$
5. V_{su} = volume of Suisun Bay, 6.54e11 L

Further explanation of the terms and schematic for the salinity balance are given in Fig. A.6.4.2.

Evaluation of assumptions

Assumption #1 may introduce the greatest amount of uncertainty, since Suisun Bay is not particularly well-mixed with respect to salinity (Fig. A.6.4.3). In future modeling efforts, a multi-box model, using smaller well-mixed volumes, could improve estimates of Qtide. With regards to Assumption #2, although salinity is not truly steady state during April-October, the most rapid

changes in salinity occur outside of these months and including non-steadiness in our model only changed the final k values by less than 7%. Assumption #3 appears to be the most valid. Salinity in the Sacramento and San Joaquin rivers is negligible and can be considered outside of tidal influence.

NH4 Balance

We used the resulting value of Q_{tide} in aNH4 mass balance, where the made the following assumptions:

1. Treated Suisun as a well-mixed control volume
2. Steady state
3. Tidal dispersion on upstream side (exchange with D19, 657) considered negligible
4. Assume loading from CCCSD mixes uniformly into Suisun Bay

We used the following terms on our model, and solved for $V_{su}k_{loss}C_{su}$(total losses,kg-d^{-1}) and k_{loss} (loss rate, d^{-1}):

1. C_{river}= flow-weighted average of $C_{D19}$and C_{657}
2. C_{su}= average(C_{D6}, C_{D7}, C_{D8})
3. C_{sp} = C_{D41}
4. Q_{adv} = $Q_{west} + Q_{rio}$
5. V_{su} = volume of Suisun Bay, 6.54e11 L
6. $\dot{M}_{discharge}$= $\dot{M}_{CCCSD}$+ $\dot{M}_{DDSD}$
7. Q_{tide} was solved for using the salinity balance

Further explanation of the terms and schematic for the NH4 balance are given in Fig. A.6.4.4.

Evaluation of Assumptions

NH4 concentrations at D6, D7 and D8 appear similar, supporting assumption #1 (Fig. A.6.4.5). However, this might be masking the influence of multiple NH4 sources into Suisun Bay. We hypothesize that NH4 concentrations actually decrease seaward from the Delta due to transformations/losses, but that CCCSD outfall just prior to D6 elevates concentrations to levels similar to those from Delta efflux. While the result corroborates our assumption of well-mixed Suisun, additional modeling on a finer spatial scale would likely reveal concentration gradients not captured by current monitoring. Regarding assumption #2, summertime NH4 concentrations are less variable than they are at other times of the year. On average, concentrations between

April and October vary by a factor of roughly 2, while concentrations on the entire year vary by a factor of 4. Assumption #3 has the potential to, if anything, underestimate the loading of NH4 into Suisun Bay. If we included a tidal dispersion term on the upstream end, this would bring high-NH4 waters from the Sacramento and San Joaquin rivers and would only increase the magnitude of observed losses in Suisun Bay. Lastly, assumption #4 may be overestimating the magnitude of NH4 loads from CCCSD. In order to evaluate the importance of this assumption, we performed our calculations assuming 100%, 75%, 50% and 25% of CCCSD plume mixing in Suisun Bay prior to advection downstream (see Figure 25)

Loads in exceeded loads out for all months analyzed (Figure A.4.6). On average, 75% of loads in are transformed or lost prior to flow out of Suisun Bay (either by advection or tidal flow)

Results

Loads in exceeded loads out for all months analyzed (Figure A.6.4.6). On average, 75% of loads in are transformed or lost prior to flow out of Suisun Bay (either by advection or tidal flow) (Figure 6.20). First order loss rates were estimated at 0.1-0.3 d^{-1}, even when some of CCCSD effluent is considered lost downstream to advection prior to mixing into Suisun Bay (Figure A.6.4.7).

We performed sensitivity analyses in order to evaluate the validity of some of our key assumptions. First, based on small variation of NH4 concentrations in April-October (Figure A.6.4.5), we assumed steady state conditions. As a comparison, we did a non-steady model and our resulting values for k vary by less than 7%, indicating that our steady-state assumption is valid. Secondly, the most uncertain term in our mass balance is the tidal flow, which we calculated using a salinity balance that itself contained simplifying assumption. We performed a sensitivity analysis in order to evaluate the effect of this parameter on our overall results. We found that if our value for tidal flow was off by a factor of 5, the contribution of transformations/losses to the overall fate of NH4 dropped from 75% to 60%, which would still be a significant contribution.

Additional discussion of results are summarized in the main body of the report (Section 6.4.3)

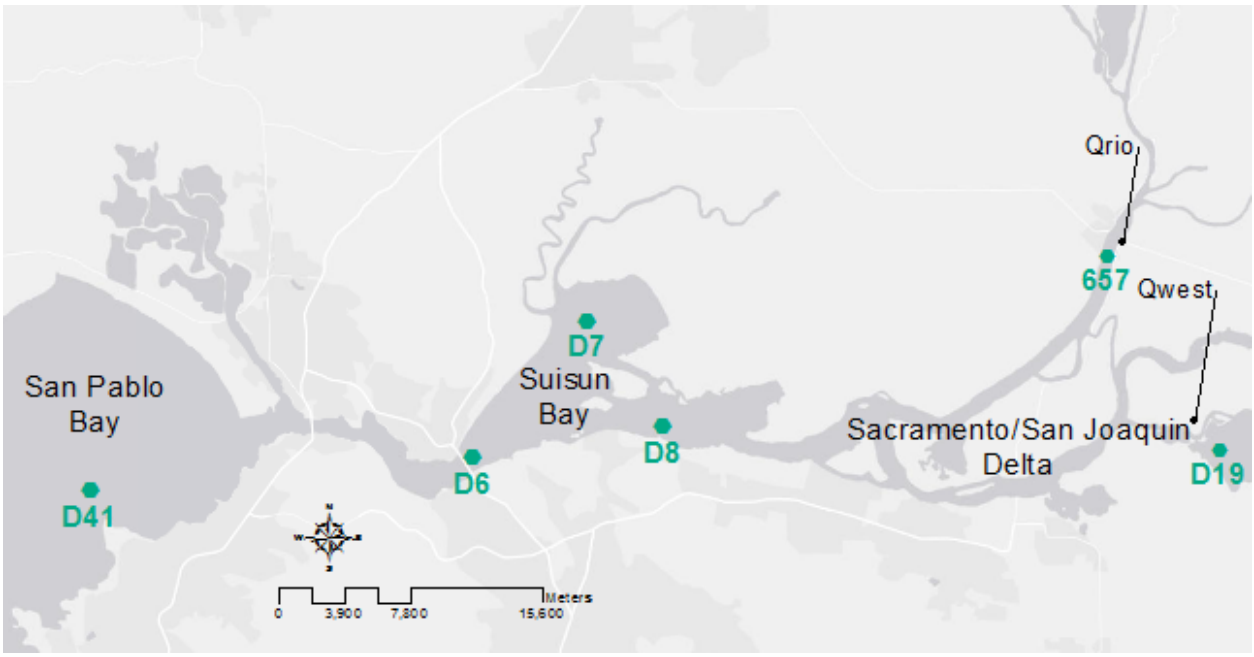

Figure A.6.4.1 Location of DWR/IEP and USGS monitoring stations (used as concentration terms) and DWR DAYFLOW stations (used as flow terms) in 1-box model for Suisun Bay. Tidal flows were estimated from a salinity balance (Fig. A.6.4.2).

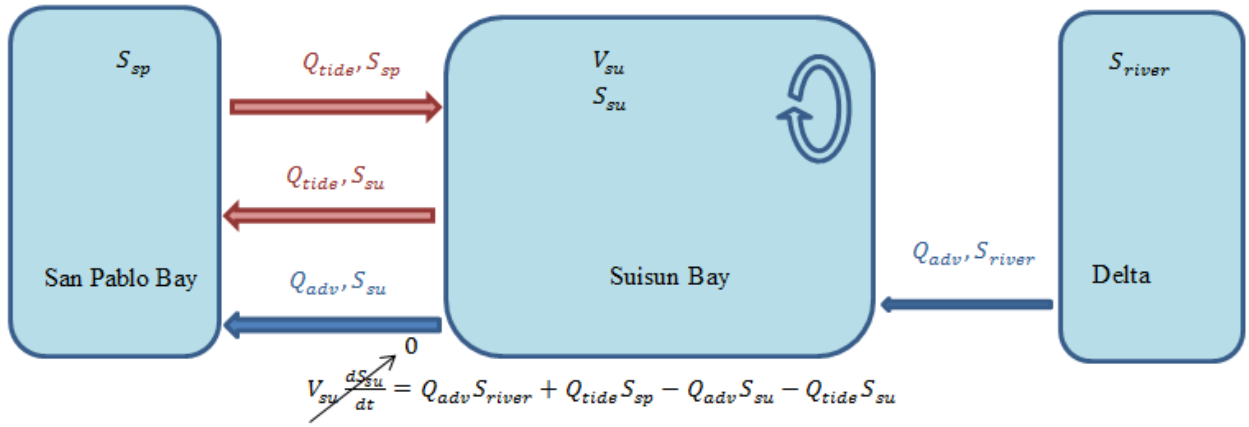

Figure A.6.4.2 Salinity mass balance schematic used to approximate the magnitude of Q_{tide}.

1. S_{river} = flow-weighted average of S_{D19} and S_{657}
2. S_{su} = average(S_{D6}, S_{D7}, S_{D8})
3. $S_{sp} = S_{D41}$
4. $Q_{adv} = Q_{west} + Q_{rio}$
5. V_{su} = volume of Suisun Bay, 6.54e11 L

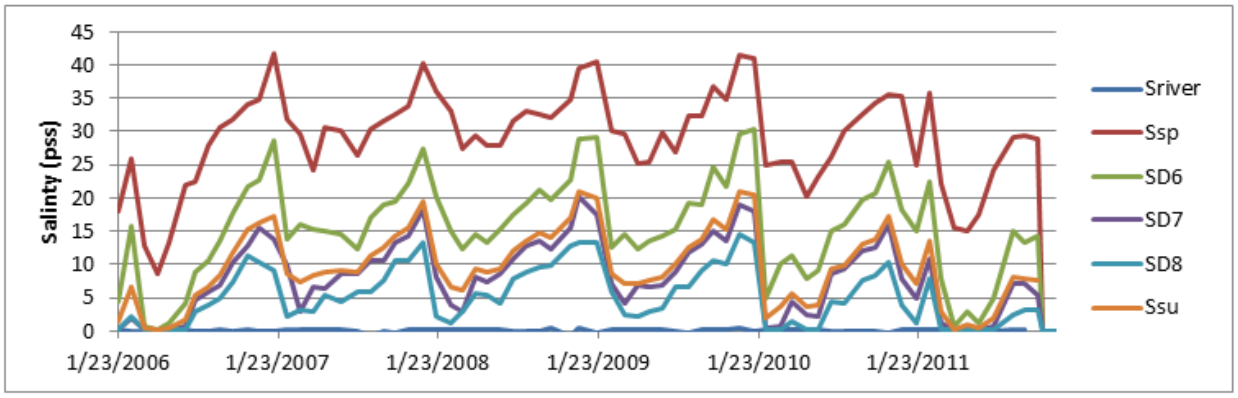

Figure A.6.4.3 Times series of salinity at locations used in mass balance (Only April-October were considered for the mode). S_{river} is the flow weighted average of salinity at DWR/IEP D19 (San Joaquin River dominated) and USGS 657 (Sacramento River dominated), S_{sp} is salinity at DWR/IEP D41 and S_{su} is the average of salinity at DWR/IEP D6, D7 and D8. This figure shows that Suisun Bay is not particularly well mixed with respect to salinity and making a well-mixed assumption may introduce uncertainty. S_{river} was negligible and therefore we neglected tidal dispersion on the upstream end of Suisun Bay

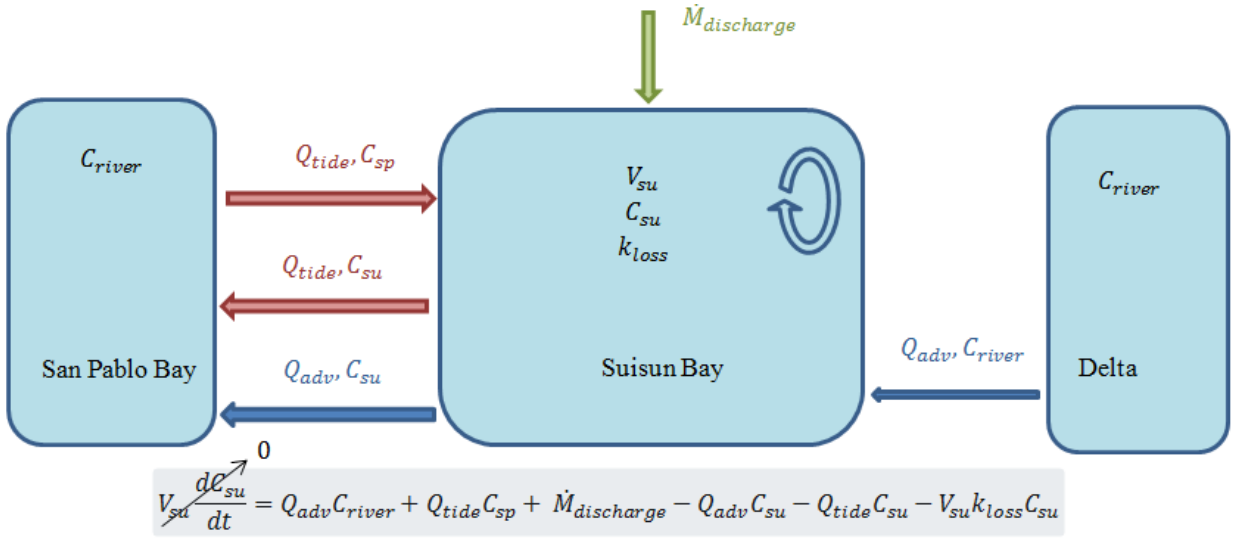

Figure A.6.4.4 Salinity mass balance schematic used to approximate the magnitude of NH4 losses in Suisun Bay.

1. C_{river}= flow-weighted average of $C_{D19}$and C_{657}
2. C_{su}= average($C_{D6,}$ C_{D7}, C_{D8})
3. C_{sp} = C_{D41}
4. Q_{adv} = $Q_{west} + Q_{rio}$
5. V_{su} = volume of Suisun Bay, 6.54e11 L
6. $\dot{M}_{discharge}$= $\dot{M}_{CCCSD}$+ $\dot{M}_{DDSD}$
7. Q_{tide} was solved for using the salinity balance

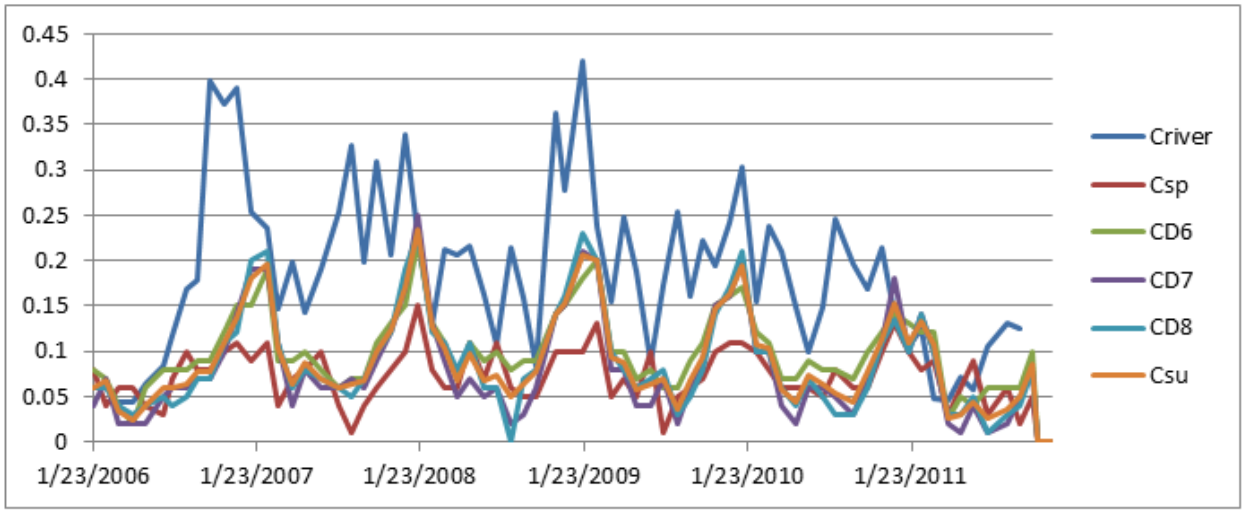

Figure A.6.4.5 NH4 concentrations at locations used in mass balance. C_{river} is the flow weighted average of NH4 at DWR/IEP D19 (San Joaquin River dominated) and USGS 657 (Sacramento River dominated), C_{sp} is NH4 at DWR/IEP D41 and C_{su} is the average of NH4 at DWR/IEP D6, D7 and D8. NH4 is reasonably well-mixed with respect to salinity. In our calculation, we neglected upstream dispersion in Suisun Bay (see Figure A.6.4.3), however given the high concentrations of NH4 in the rivers, if anything this omission underestimates NH4 loads to Suisun Bay and therefore underestimates the magnitude of NH4 losses.

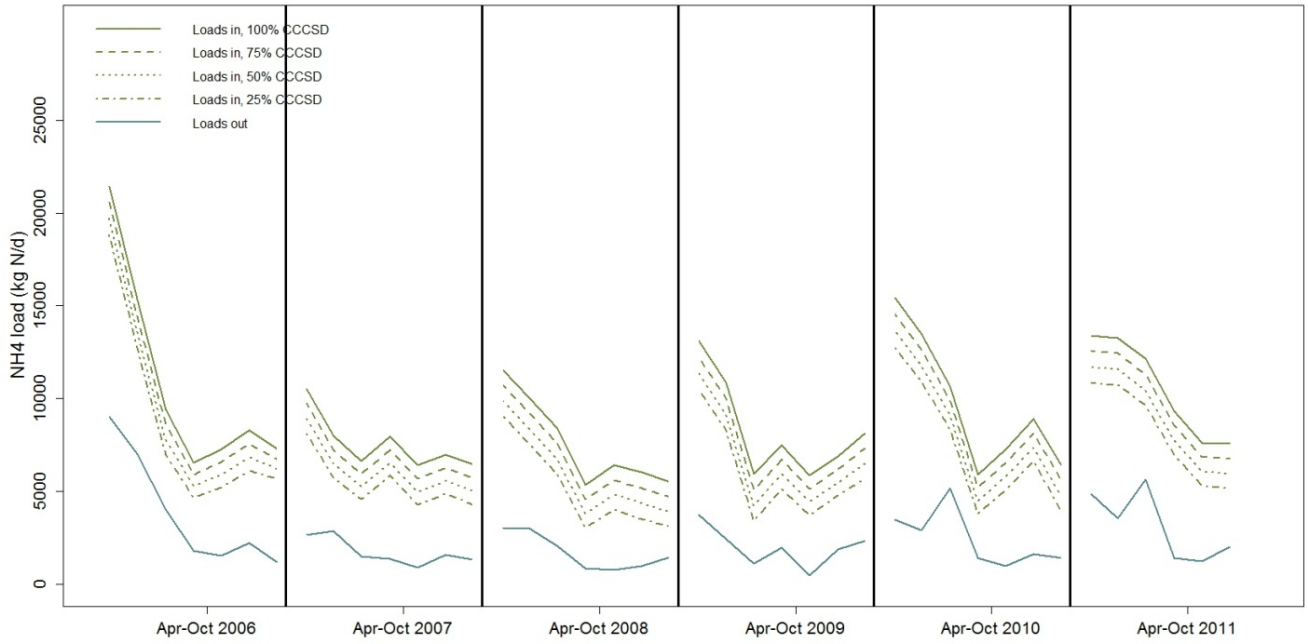

Figure A.6.4.6 Differences between NH4 loads into Suisun Bay (including advective loads, tidal downstream tidal loads and discharger loads assuming various amounts of CCCSD effluent mixing; green line) and NH4 loads out of Suisun Bay (including advective loads and downstream tidal loads). The difference between loads in and loads is an estimate of the magnitude of NH4 losses in Suisun Bay (kg d^{-1}). Even when only 25% of CCCSD plume was allowed to mix into Suisun Bay prior to advecting downstream, loads in always exceeded loads out by as much as 2-3 times. First-order loss rates are presented in Fig. A.6.4.7.

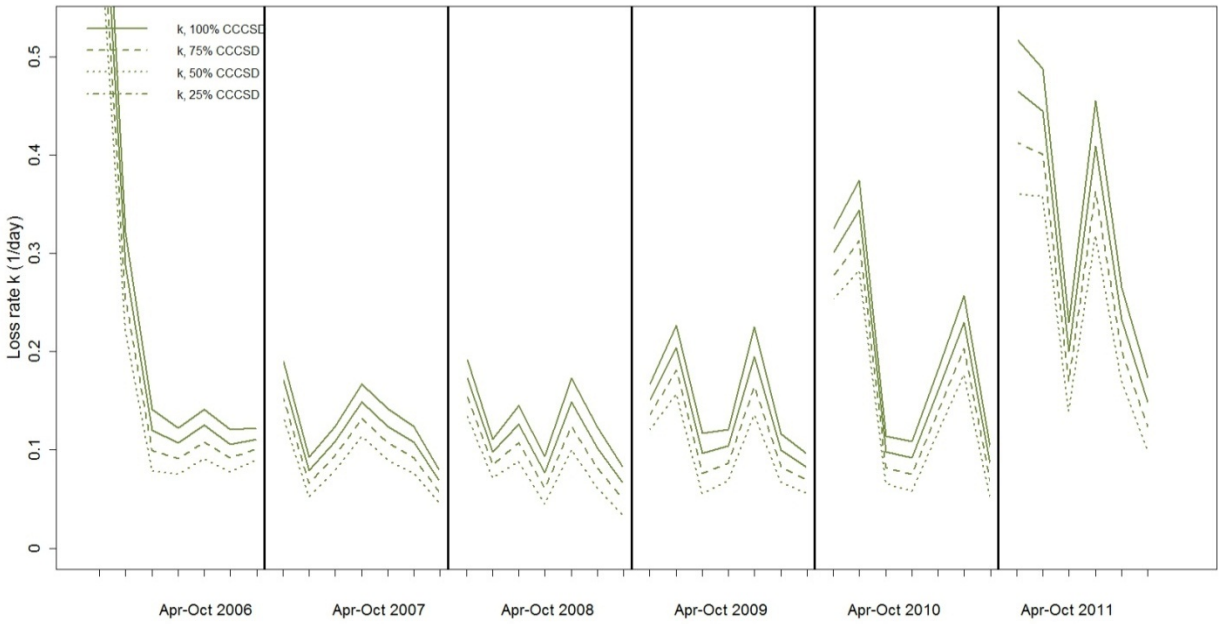

Fig A.6.4.7 Estimated first order loss rates for NH4 in Suisun Bay during low-flow periods in Suisun Bay. Loss rates were approximated by a 1-box mass balance that considered advective loads in, downstream tidal loads in, discharger loads in, advective loads out and downstream tidal loads out of Suisun Bay. Due to the location of CCCSD discharge, it is likely that some of the effluent plume may be advected downstream prior to mixing into Suisun Bay, so the model was run assuming a range of CCCSD effluent mixing into Suisun Bay.